Transport-Based Modeling of Bubble Nucleation on Gas Evolving Electrodes

Transport-based modeling of bubble nucleation on gas evolving electrodes

Zhengmao Lu[1a], Lenan Zhang[2a], Ryuichi Iwata[2], Evelyn N. Wang[2*], Jeffrey C. Grossman[1*]

[1] Department of Materials Science and Engineering, Massachusetts Institute of Technology, Cambridge, MA 02139, USA

[2] Department of Mechanical Engineering, Massachusetts Institute of Technology, Cambridge, MA 02139, USA

[*] Corresponding author: enwang@mit.edu, jcg@mit.edu

[a] These authors contributed equally

Abstract

Bubble nucleation is ubiquitous in gas evolving reactions which are instrumental for a variety of electrochemical systems. Fundamental understanding of the nucleation process, which is critical to system optimization, remains limited as prior works generally focused on the thermodynamics and have not considered the coupling between surface geometries and different forms of transport in the electrolytes. Here, we establish a comprehensive transport-based model framework to identify the underlying mechanism for bubble nucleation on gas evolving electrodes. We account for the complex effects on the electrical field, ion migration, ion diffusion, and gas diffusion arising from surface heterogeneities and gas pockets initiated from surface crevices. As a result, we show that neglecting these effects leads to significant underprediction of the energy needed for nucleation. Our model provides a non-monotonic relationship between the surface cavity size and the overpotential required for nucleation, which is physically more consistent than the monotonic relationship suggested by a traditional thermodynamics-based model. We also identify the significance of the gas diffuse layer thickness, a parameter controlled by external flow fields and overall electrode geometries, which has been largely overlooked in previous models. Our model framework offers guidelines for practical electrochemical systems whereby without changing the surface chemistry, nucleation on electrodes can be tuned by engineering the cavity size and the gas diffuse layer thickness.

Introduction

Gas evolving electrodes play a critical role in many industrial scale electrochemical reactions including water splitting,[1] sodium chlorate production,[2] and chloralkaline processes.[3] It is well-known that bubble formation on electrodes often causes higher electrolyte transport resistances, which is detrimental to overall system efficiencies.[4] Meanwhile, bubble-based electrolytic cleaning has proved useful for defouling of membranes in water purification, where more bubble generation is desired.[5,6] A fundamental understanding of nucleation on gas evolving electrodes is crucial to optimizing these different electrochemical systems, and yet a complete understanding of the nature of bubble formation as well as the associated transport physics is still lacking. Although it is possible for bubbles to form homogeneously in bulk solutions, in practice, heterogenous nucleation from surface cavities is more common as the energy barrier is lower (Fig. 1a).[7] Nevertheless, previous models for bubble nucleation on gas evolving electrodes have largely overlooked the interaction between surface geometries and various transport mechanisms. Ward *et al*. demonstrated the thermodynamic foundation of gas nucleation where they determined the critical bubble size as a function of gas concentration.[8] While the theory was initially derived for spherical bubbles in the bulk, Luo *et al.* and German *et al.* applied Ward *et al*.'s framework to surface bubbles after accounting for the contact angle effect and shed light upon the nucleation process with experimental nanoelectrode tests.[9–11] However, the role of surface cavities were not explicitly considered. On the other hand, Atchley and Properetti[12] presented a crevice model for acoustic bubble nucleation, which was further developed by Borkent *et al*.[13] Lohse and Zhang discussed the stabilization of surface nanobubbles by contact line pinning.[14] Volanschi *et al*. investigated the effect of cavities on the reacting surface, assuming uniform reaction rates on the electrode.[15] This assumption, however, ignores the complicated effects of surface heterogeneities on electrical fields, ion diffusion and migration, and electrochemical reactions (Fig. 1b). Moreover, once initiated from the cavity, a nascent bubble immediately blocks part of the electrode area and starts diffusing into the bulk due to the Laplace pressure,[16] affecting whether this bubble will grow or collapse. To comprehensively account for the effects of surface geometries and the potential presence of a bubble, here we develop a transport-based nucleation model framework. We quantify the relationship between the overpotential and the critical bubble radius, where we identify a cavity size that requires the minimum activation energy to trigger nucleation given an electrode-solution pair and a working

condition. Our model suggests that the conventional thermodynamics approach significantly underestimates the activation overpotential when the cavity size is comparable to the gas diffuse layer thickness. Rather than modifying the surface chemistries, we show that the electrochemical process can be tuned through nucleation control by physically engineering electrode geometries and the gas diffuse layer thickness.

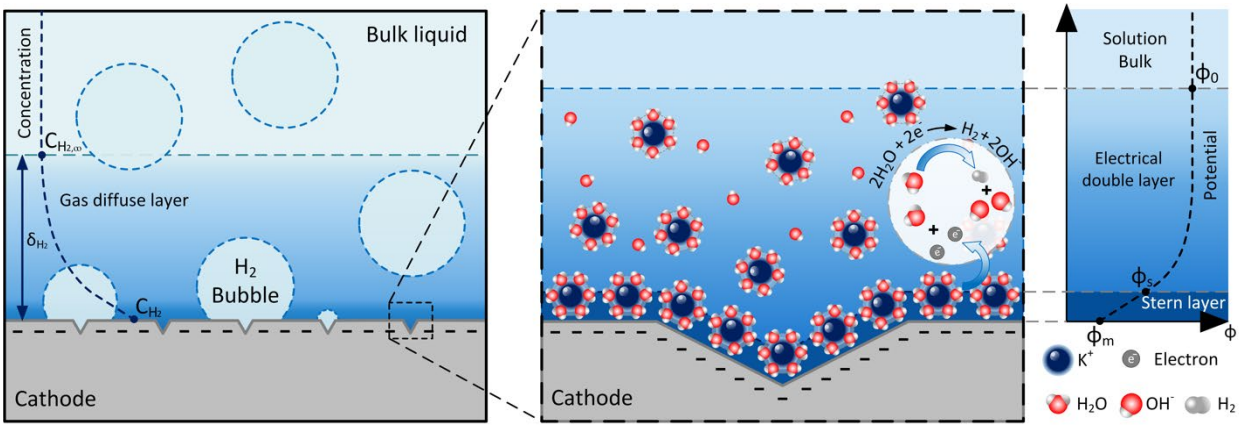

Fig. 1 Schematic describing the physical picture of bubble nucleation from hydrogen evolving electrodes in alkaline solutions. (a) Gas bubble nucleating from surface cavities where gas concentration is higher. The gas diffusion resistance between the electrode and the bulk is characterized by the gas diffuse layer thickness δ_{H_2}. (b) Chemical reaction, ion migration, and diffusion in the electrical double layer of which the thickness is on the order of the Debye length.

Model Formulation

Our model focuses on the effect of surface cavities and the presence of gas pockets initiated from surface crevices on gas diffusion, ion migration and diffusion, and electrochemical reaction. Each transport mechanism by itself has been relatively well-understood: the gas diffusion follows Fick's law;[17] the ion transport is governed by the Nernst-Planck equation;[18] and the kinetics of electrochemical reactions can usually be described by the Tafel equation at large overpotentials.[19] Nevertheless, the coupling between different forms of transport have not been comprehensively modeled in previous nucleation studies. Here, we show that these transport phenomena greatly affect the bubble formation process. To detail the current model framework, we take alkaline water electrolysis as an example, which is one of the most popular methods for hydrogen production. The framework that we develop here can be broadly applied to other gas evolving reactions as well with different sets of electrochemical reaction kinetics and electrolyte properties. We consider a hydrogen evolving cathode surface in a potassium hydroxide solution (Fig. 1b), where the following chemical reaction occurs:

$$H_2O + e^- \rightleftharpoons \frac{1}{2}H_2 + OH^- \quad (1)$$

The net rate of this reaction is characterized by the cathodic current density j, which is related to the kinetic overpotential η_s, often in the form of the Tafel equation when η_s is large enough:

$$\eta_s = \eta_0 \log_{10}\left(\frac{j}{j_0}\right) \quad (2)$$

where j_0 is the exchange current density and η_0 is the so-called Tafel slope. Both j_0 and η_0 depend on electrode materials and system temperatures.[20] In our simulation, we consider j_0 = 0.1 A and η_0 = 120 mV, which falls within the range of previous experiments.[1] The plane that passes through the centers of solvated ions adsorbed onto the electrode is defined as the outer-Helmholtz plane (OHP), which is usually considered to be the surface where charge transfer occurs. Between the OHP and electrode surface is the Stern layer across which η_s is calculated.[21] Based on charge conservation, we can express the molar flux/reaction rate for OH^- (k) and H_2 (k_{H_2}) into the electrolyte as:

$$k = \frac{j}{F} \quad (3)$$

and

$$k_{H_2} = \frac{k}{2} = \frac{j}{2F} \quad (4)$$

where F is the Faraday constant. We set the bulk solution to be 0.1 M KOH saturated with H_2 ($C_{H_2,\infty}$ = 0.8 mM), consistent with typical experimental working conditions.[1] To model the steady-state transport of different species, we use mass conservation:

$$\nabla \cdot \mathbf{J}_i = 0, \qquad i = K^+, OH^-, H_2 \quad (5)$$

where $\mathbf{J}_i$ is the molar flux vector and can be expanded as

$$\mathbf{J}_i = -D_i \nabla C_i - \frac{D_i C_i z_i F}{RT} \nabla \phi. \quad (6)$$

The first term on the right-hand side corresponds to mass diffusion and the second term describes ion migration under the electrical field. Here, D_i, C_i and z_i are the diffusion coefficient, molar concentration, and charge of species i, respectively. R is the universal gas constant, T is the system temperature (which we set to be 25 °C), and ϕ is the electric potential determined from the Poisson equation:

$$\nabla \cdot (\epsilon_0 \epsilon_r \nabla \phi) = -F \Sigma z_i C_i \quad (7)$$

where ϵ_0 is the vacuum permittivity and ϵ_r is the relative permittivity of water. For the electrical field boundary conditions, while we assume $\phi = 0$ in the bulk, the potential at the electrode ϕ_m is our model input. We assume a Stern layer thickness of $\lambda_s = 0.5$ nm[21,22] and calculate η_s as:

$$\eta_s = \phi_s - \phi_m = -\lambda_s \mathbf{n} \cdot [\nabla \phi]_{OHP} \quad (8)$$

where ϕ_s is the electrical potential at the OHP. For the mass transfer boundary to the bulk, we note the difference between the gas diffuse layer and the electrical double layer (EDL). The thickness of the EDL is characterized by the Debye length:

$$\lambda_D = \sqrt{\frac{\epsilon_0 \epsilon_r RT}{2F^2 I}} \quad (9)$$

where I is the molar ionic strength. For a monovalent binary electrolyte like KOH, I takes the same value as the bulk cation (K^+) concentration, which results in $\lambda_D = 0.96$ nm. The EDL is a boundary layer of charged species induced by the electrical field. Meanwhile, there is another boundary layer resulted from diffusion and fluid mechanics for all species, δ_i which scales with $(D_i/\nu)^{1/3}$ ($i = K^+$, OH^-, and H_2).[23,24] Here, ν is the kinematic viscosity of the solution and δ_i, determined by the overall electrode size and external flow field, is usually significantly larger than λ_D. This implies that the major variation of the ion concentration occurs within the EDL (Figure S1) while the concentration of gas molecules which are neutral in the electrical field has a smoother change over a longer distance (δ_{H_2}). Beyond the gas diffuse layer, we assume the dissolved gas concentration to take bulk values. In this study, we consider an axisymmetric simulation domain with a cone-shape cavity in the middle, which includes the whole gas diffuse layer. For the reference case, we set $\delta_{H_2} = 1$ μm, the cavity radius $r_{cav} = 5\lambda_D$, and the cone half angle $\theta = 45°$ (Fig. 2 a and b). The parameters used in this study are summarized in Table S1. We note that the natural convection effect and the gas depletion effect are not included in the current model as we have focused on the initial stage of bubble nucleation and the maximum bubble radius considered is < 1 μm. These effects can become important for larger bubbles (> 20 μm) and after bubbles detach from the surface.[25] We ensure that the simulation cell radius is large enough ($r_{cell} = 6r_{cav}$) to minimize side boundary effects (Figure S2). Equations (1)-(8) are then solved in the electrolyte region using the finite element methods with COMSOL Multiphysics. (See Figure S3 and S4 for mesh sensitivity test.) We benchmark our diffusion solver with a simulation result reported by Luo and White,[9] where they modeled the proton

diffusion limited current on a Pt nanoelectrode partially covered by a bubble (Figure 6c in ref. 9). We replicated their results in Fig. 2, where good agreement is shown.

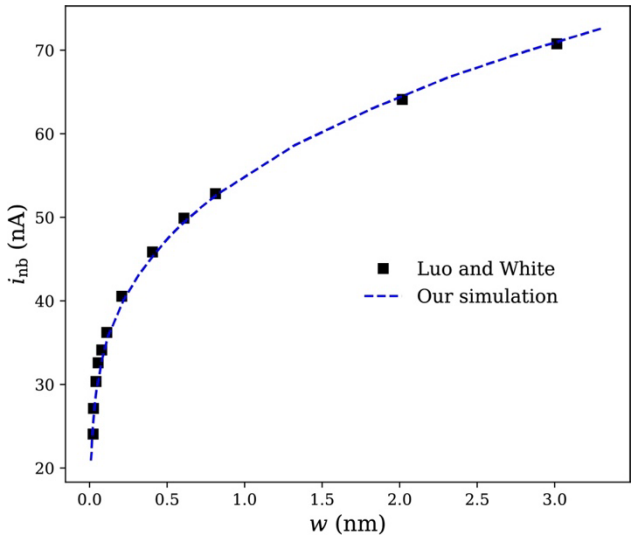

Fig. 2 Benchmark simulation (blue dashed line) against results reported by Luo and White (black solid squares).[9] Proton diffusion limited current i_{nb} is plotted as a function of the exposed width w of a Pt nanoelectrode partially covered by a bubble. More details can be found in Figure 6c in ref. 9.

Results and Discussion

Figure 3 shows the electrical potential and gas concentration profile for $20\lambda_D$ into the electrolyte solution (part of the simulation region) with reference working conditions at ϕ_m = -900 mV. In Fig. 3a, most of the potential change occurs very close to the electrode surface as the ion diffuse layer is much thinner than the gas diffuse layer. With the solved electrical potential profile, we can calculate the potential difference across the Stern layer η_s and the surface reaction rate k, which we normalize to the Tafel slope η_0 and the reference reaction rate $k_0 = j/F$, respectively. These two quantities are related by Eq. (2) and Eq. (3), shown in the double-axis plot in Fig. 3b as a function of the r-coordinate (distance to the center axis). We select a few values of ϕ_m which are consistent with typical experimental conditions in literature.[19,26] We note that the reaction rate always starts low at point A and peaks at point B, which is simply due to the variation of the local electrical field strength (η_s/λ_s). Interestingly, the location where k is the highest does not have the highest gas concentration, as shown in Fig. 3c and 3d. In Fig. 3c, we observe that near the electrode, the gas concentration C_{H_2} much exceeds the bulk saturation value $C_{H_2,\infty}$. Due to the larger reaction area per unit volume near the bottom of the cavity, the highest C_{H_2} appears at point A although the reaction rate at that location is the lowest. This result becomes more

obvious as we plot the normalized gas concentration $C_{H_2}/C_{H_2,\infty}$ as a function of the r-coordinate along the electrode in Fig. 3d. The cavity gas concentration increases even more as we decrease the cone half angle θ, where the values of θ are selected based on surface cavities fabricated in previous heterogeneous nucleation studies.[27,28] These results suggest that nucleation will occur first from the cavity simply based on the gas concentration profile, consistent with previous studies.[15] The sharper the cone half angle, the more prone the cavity is to nucleate.

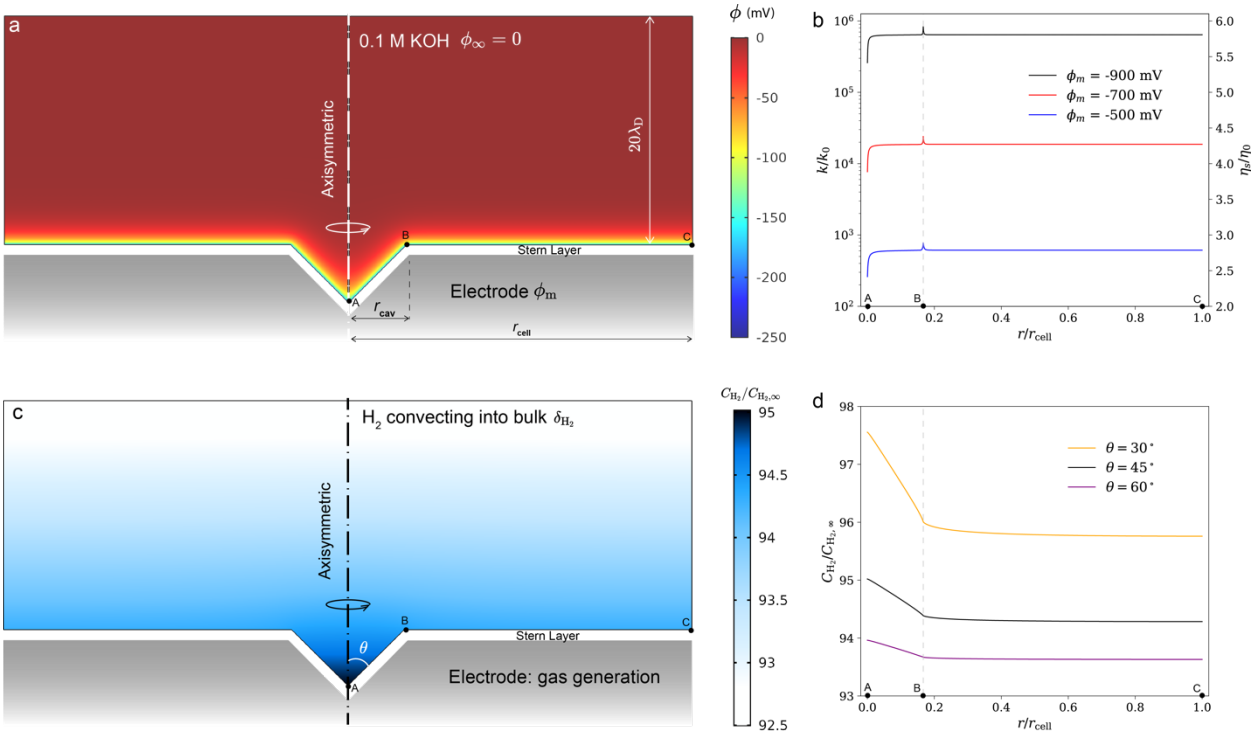

Fig. 3 Electrical potential and gas concentration profile. (a) Contour plot of electrical potential profile near the electrode for ϕ_m = -900 mV, θ = 45°, r_{cav} = 5λ_D, and δ_{H_2}=1 μm. Stern layer thickness is not drawn to scale. (b) Normalized reaction rates k/k_0 and kinetic overpotential η_s/η_0 as a function of the r-coordinate along the electrode for select values of ϕ_m. The kink at point B is caused by discontinuities of surface curvatures. (c) Contour plot of dissolved gas concentration near the electrode for ϕ_m = -900 mV, θ = 45°, r_{cav} = 5λ_D, and δ_{H_2}=1 μm. Note that the gas diffuse layer is much larger than the region shown. (d) Normalized gas concentration as a function of the r-coordinate along the electrode for select values of θ.

Based on the gas concentration on the electrode, a previous thermodynamics-based model predicts a critical nucleation radius[16]:

$$r_{c,therm} = \frac{2\gamma}{P_0\left(\frac{C_{H_2,B}}{C_{H_2,\infty}} - 1\right)} \tag{10}$$

where γ is the surface tension of the liquid-gas interface, P_0 is the ambient pressure. Here, we use $C_{H_2,B}$, the gas concentration at point B, to represent the gas concentration near the cavity. We find

that $C_{H_2,B}$ is very sensitive to the gas diffuse layer thickness δ_{H_2}, which largely determines the mass transfer resistance of the dissolved gas from the electrode to the bulk.

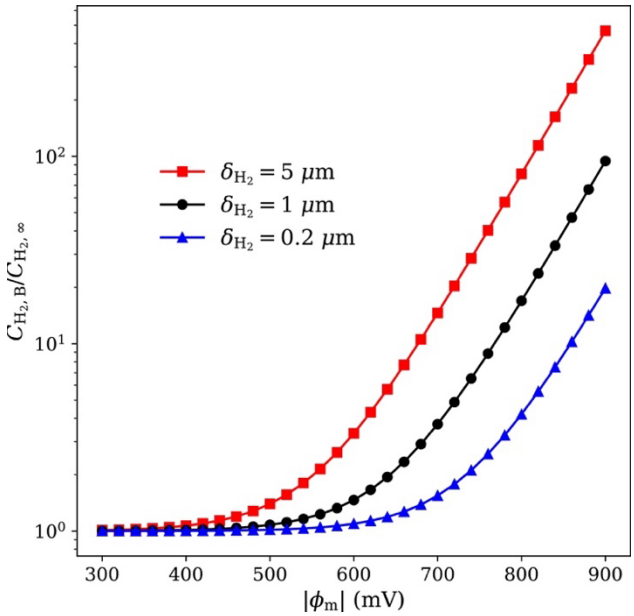

Fig. 4 Normalized gas concentration near the cavity $C_{H_2,B}/C_{H_2,\infty}$ as a function of the magnitude of potential applied to the electrode for select values of gas diffuse layer thickness δ_{H_2}.

In Fig. 4, $C_{H_2,B}/C_{H_2,\infty}$ is plotted as a function of the magnitude of electrical potential applied to the electrode $|\phi_m|$ for select values of δ_{H_2} (0.2 μm, 1 μm, and 5 μm) which are representative for experimental conditions in previous studies of gas evolving electrodes.[10,29–31] The increase of $|\phi_m|$ causes higher chemical reaction rates, which leads to higher $C_{H_2,B}$. Meanwhile, decreasing δ_{H_2} facilitates gas diffusion into the bulk solution, which gives rise to lower gas concentration at the electrode. By relating $C_{H_2,B}/C_{H_2}$ to $|\phi_m|$ and using Eq. (10), we obtain the thermodynamics-based prediction for the necessary electrical potential to activate nucleation given a critical bubble radius (blue dashed line for δ_{H_2} = 0.2 μm and black dashed line for δ_{H_2} = 1 μm in Fig. 5a). This thermodynamics-based approach suggests that nucleation of larger bubbles can always take place with lower $|\phi_m|$. In other words, given a $|\phi_m|$ from which we can find an associated r_c, all cavities with radii greater than r_c can be activated. However, in practical experiments, this thermodynamics-based prediction is not necessarily valid since macroscale cavities rarely promote nucleation and there is an upper limit for the size of bubbles that can be generated from surface crevices. To resolve this discrepancy, we consider the potential effect of the presence of the bubble itself on the nucleation process. Once a nascent gas bubble is initiated from a cavity,

it immediately blocks part of the reaction area and the bubble growth is supported by the rest of the reactive region (Fig. 5b). Meanwhile, since the internal bubble pressure P_b is higher than ambient pressure P_0 due to the Laplace pressure, gas diffuses away from the bubble into the bulk. Depending on the net gas flux at the interface, the bubble can either grow out of the cavity or collapse back after initiation. Accordingly, we establish a new criterion for bubble nucleation on gas evolving electrodes from this transport perspective.

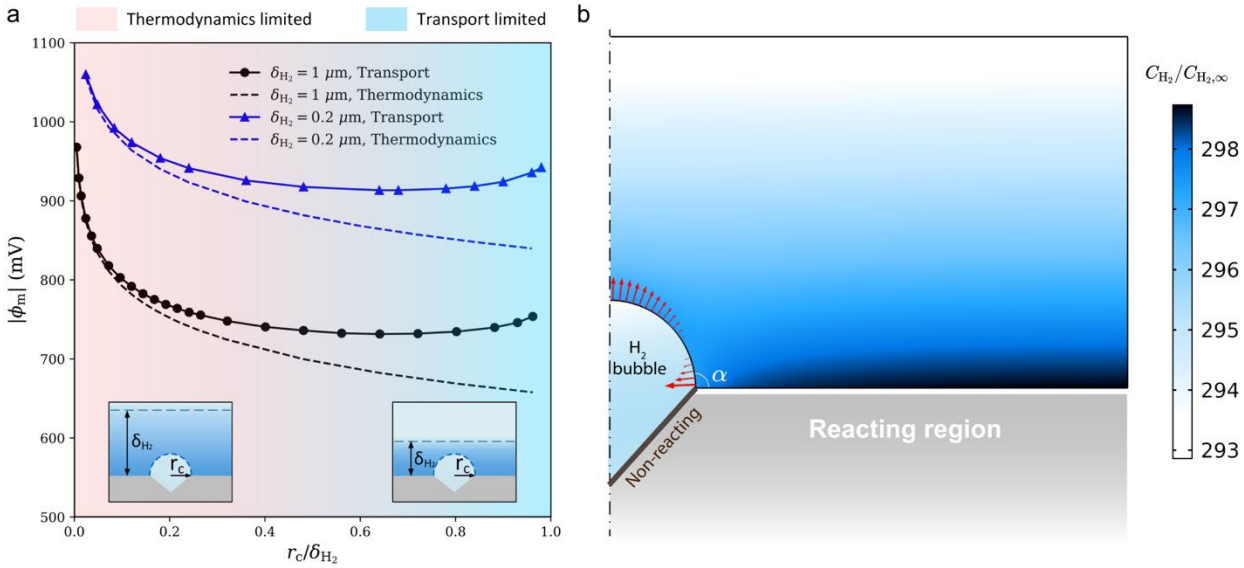

Fig. 5 Effect of presence of the bubble on the nucleation process. (a) Magnitude of electrical potential applied to electrodes as a function of the ratio between critical bubble radius r_c and gas diffuse layer thickness δ_{H_2} predicted by the conventional thermodynamics-based model (blue dashed line for δ_{H_2} = 0.2 μm and black dashed line for δ_{H_2} = 1 μm) and the current transport-based model (black dots for δ_{H_2} = 1 μm and blue triangles for δ_{H_2} = 0.2 μm). (b) Normalized hydrogen concentration in the electrolyte solution with a nascent gas bubble pinned at the cavity covering part of the electrochemical reaction area (α = 90°). The length of red arrows is proportional to diffusive gas fluxes along the interface. In this simulation, ϕ_m = -967.9 mV, θ = 45°, r_{cav} = 5λ_D, and δ_{H_2}=1 μm, which results in zero net hydrogen flux across the interface.

Note that as the bubble continues to grow, the three-phase contact line experiences pinning at the top corner of the cavity. We consider the critical point where the contact angle α = 90°, corresponding to the largest P_b during the pinning process. At this point, according to the Young-Laplace equation,

$$P_b - P_0 = \frac{2\gamma}{r_{cav}} \tag{11}$$

and the saturation gas concentration under P_b is

$$C_{H_2,in} = K_H P_b \tag{12}$$

where K_H is the Henry's solubility constant for H_2 in water. We assign $C_{H_2,in}$ at the liquid-gas interface and calculate the net gas molar flux into the bubble j_b. If $j_b > 0$, the bubble can grow out of the cavity; if $j_b < 0$, then the bubble collapses. For a given r_c, using this transport-based model, $|\phi_m|$ is calculated as the magnitude of the overpotential that leads to $j_b = 0$. For example, in Fig. 5b, we show the dissolved H_2 concentration profile with a pinned nascent gas bubble where θ = 45°, $r_{cav} = 5\lambda_D$, δ_{H_2}=1 μm and α = 90°. The net flux across the interface becomes zero as we set the electrode potential to be -967.9 mV, from which we obtain that $r_c = 5\lambda_D$ when $|\phi_m|$ = -967.9 mV (Figure S5). In Fig. 5a, predictions of the relationship between r_c and $|\phi_m|$ are plotted in black dots for δ_{H_2} = 1 μm and blue triangles for δ_{H_2} = 0.2 μm using the transport-based model. For small r_c/δ_{H_2} (< 0.1), the top of the bubble is still far away from the gas diffusion boundary, which makes the diffusive flux from the bubble into the bulk solution insignificant. The $j_b = 0$ criterion then reduces to requiring gas concentration at the exposed electrode to be around $C_{H_2,in}$, which is similar to the thermodynamics result. Consequently, predictions from the two models are very close to each other in this regime, which helps support the results of our transport-based model. As r_c/δ_{H_2} becomes larger (> 0.4), the diffusion into the bulk cannot be ignored anymore and there are concentration gradients from the exposed electrode to the bubble to balance this outflux. As a result, the thermodynamics-based model largely underestimates the $|\phi_m|$ required to activate a bubble compared to the transport-based model. The point where this transition starts becoming more apparent is mostly determined by the transport resistance contrast between gas supply from the electrode and gas diffusion into the bulk. When r_c/δ_{H_2} approaches unity, the transport-based model suggests that it requires more overpotential to activate larger bubbles as the upper portion of the bubble grows deeper into the relatively low gas concentration region. Under a certain set of working conditions, this in turn sets an upper limit of r_c for a given $|\phi_m|$, resolving the previous inconsistencies in the thermodynamics-based model. Note that the range of values set for r_c at a certain $|\phi_m|$ corresponds to the bubble nucleation stage. The actual bubble size observed in experiments also depends on the bubble growth and the bubble detaching process, which are not considered in the current study. Further, we identify a minimum of the activation overpotential at a r_c/δ_{H_2} between 0.6 and 0.7. The cavity radius for the minimum activation overpotential r_c^* also depends on the electrode-solution pair as well as other working conditions such as the temperature. Nevertheless, given a particular system, to promote nucleation, we can add artificial cavities of radii close to this r_c^* onto the electrode surface. On

the other hand, when bubbles are undesired, one can create surface cavities far away from this size, which leads to a higher overpotential required for nucleation but still increases the effective reaction area. Moreover, controlling the gas diffuse layer thickness is also critical to optimizing the nucleation process as well, which has not received much attention in prior works. The gas diffuse layer can be thinned down by using smaller sized electrodes or increasing the flow speed in the bulk solution (e.g., with stirring or cross-flow setups). This provides pathways to verifying the findings in our model as one can experimentally vary δ_{H_2} and monitor the associate change in the minimum activation potential. The experimental validation of our model certainly warrants further studies. Thinner δ_{H_2} results in more effective diffusive transport while impeding bubble generation. For example, in our case study, reducing δ_{H_2} by 80% caused the minimum activation overpotential to increase by around $1.5\eta_0$. Overall, the fundamental understanding obtained from the transport-based model offers insights into designing practical electrochemical systems.

Conclusion

We established a transport-based model framework for bubble nucleation on gas evolving electrodes, where we accounted for coupling between surface geometries, electrostatics, electrochemical reaction, ion migration, ion diffusion, and gas diffusion. More importantly, we modeled the potential effect of nascent bubbles initiated from surface crevices. We considered the balance between gas diffusion from the bubble to the bulk solution and gas supplied to the bubble from the reacting area of the electrode. As a result, we set up a criterion for bubble nucleation from a transport perspective. We found that the traditional thermodynamics-based model significantly underestimates the overpotential required for activating cavities of sizes comparable to the gas diffuse layer thickness. While the thermodynamics analysis suggested a monotonic relationship between the cavity size and activation overpotential, our transport-based model shows that nucleation requires more energy when the nascent bubble size is either too small or too large. As much of the optimization of electrochemical processes has focused on modification of electrode surface chemistry, we have illustrated the importance of transport in the electrolyte solution. Our model provides design guidelines for practical systems, which suggests that bubble nucleation, a key process in gas evolving reactions, can be tuned through engineering the surface cavity size and the gas diffuse layer thickness.

Reference

1. Zeng, K. & Zhang, D. Recent progress in alkaline water electrolysis for hydrogen production and applications. *Prog. Energy Combust. Sci.* **36**, 307–326 (2010).
2. Viswanathan, K. Chemical, Electrochemical, and Technological Aspects of Sodium Chlorate Manufacture. *J. Electrochem. Soc.* **131**, 1551 (1984).
3. Hou, M. *et al.* A clean and membrane-free chlor-alkali process with decoupled Cl2 and H2/NaOH production. *Nat. Commun.* **9**, (2018).
4. Angulo, A., van der Linde, P., Gardeniers, H., Modestino, M. & Fernández Rivas, D. Influence of Bubbles on the Energy Conversion Efficiency of Electrochemical Reactors. *Joule* **4**, 555–579 (2020).
5. Wu, Z. H. *et al.* Cleaning using nanobubbles: Defouling by electrochemical generation of bubbles. *J. Colloid Interface Sci.* **328**, 10–14 (2008).
6. Lalia, B. S., Ahmed, F. E., Shah, T., Hilal, N. & Hashaikeh, R. Electrically conductive membranes based on carbon nanostructures for self-cleaning of biofouling. *Desalination* **360**, 8–12 (2015).
7. Jones, S. F., Evans, G. M. & Galvin, K. P. Bubble nucleation from gas cavities - A review. *Adv. Colloid Interface Sci.* **80**, 27–50 (1999).
8. Ward, C. A., Balakrishnan, A. & Hooper, F. C. On the thermodynamics of nucleation in weak gas-liquid solutions. *J. Fluids Eng. Trans. ASME* **92**, 695–701 (1970).
9. Luo, L. & White, H. S. Electrogeneration of single nanobubbles at sub-50-nm-radius platinum nanodisk electrodes. *Langmuir* **29**, 11169–11175 (2013).
10. German, S. R., Edwards, M. A., Ren, H. & White, H. S. Critical Nuclei Size, Rate, and Activation Energy of H2 Gas Nucleation. *J. Am. Chem. Soc.* **140**, 4047–4053 (2018).
11. German, S. R. *et al.* Electrochemistry of single nanobubbles. Estimating the critical size of bubble-forming nuclei for gas-evolving electrode reactions. *Faraday Discuss.* **193**, 223–240 (2016).
12. Atchley, A. A. & Prosperetti, A. The crevice model of bubble nucleation. *J. Acoust. Soc. Am.* **86**, 1065–1084 (1989).
13. Borkent, B. M., Gekle, S., Prosperetti, A. & Lohse, D. Nucleation threshold and deactivation mechanisms of nanoscopic cavitation nuclei. *Phys. Fluids* **21**, (2009).
14. Lohse, D. & Zhang, X. Surface nanobubbles and nanodroplets. *Rev. Mod. Phys.* **87**, 981–

1035 (2015).
15. Volanschi, A., Nijman, J. G. H., Olthuis, W. & Bergveld, P. Microcavity electrodes used as single-nucleation site electrodes for the electrolysis of water. *Sensors Mater.* **9**, 223–240 (1997).
16. Enríquez, O. R. *et al.* Growing bubbles in a slightly supersaturated liquid solution. *Rev. Sci. Instrum.* **84**, (2013).
17. Epstein, P. S. & Plesset, M. S. On the Stability of Gas Bubbles in Liquid-Gas Solutions. *J. Chem. Phys.* **19**, 256 (1951).
18. Zheng, Q. & Wei, G. W. Poisson-Boltzmann-Nernst-Planck model. *J. Chem. Phys.* **134**, (2011).
19. Krstajić, N., Popović, M., Grgur, B., Vojnović, M. & Šepa, D. On the kinetics of the hydrogen evolution reaction on nickel in alkaline solution - Part I. The mechanism. *J. Electroanal. Chem.* **512**, 16–26 (2001).
20. Hu, C., Zhang, L. & Gong, J. Recent progress made in the mechanism comprehension and design of electrocatalysts for alkaline water splitting. *Energy Environ. Sci.* **12**, 2620–2645 (2019).
21. Bohra, D., Chaudhry, J. H., Burdyny, T., Pidko, E. A. & Smith, W. A. Modeling the electrical double layer to understand the reaction environment in a CO2 electrocatalytic system. *Energy Environ. Sci.* **12**, 3380–3389 (2019).
22. Wang, H. & Pilon, L. Accurate simulations of electric double layer capacitance of ultramicroelectrodes. *J. Phys. Chem. C* **115**, 16711–16719 (2011).
23. Garmo, A., Naqvi, K. R., Røyset, O. & Steinnes, E. Estimation of diffusive boundary layer thickness in studies involving diffusive gradients in thin films (DGT). *Anal. Bioanal. Chem.* **386**, 2233–2237 (2006).
24. Welty, J., Rorrer, G. L. & Foster, D. G. *Fundamentals of momentum, heat, and mass transfer*. (John Wiley & Sons, 2020).
25. Enríquez, O. R., Sun, C., Lohse, D., Prosperetti, A. & Van Der Meer, D. The quasi-static growth of CO2 bubbles. *J. Fluid Mech.* **741**, 1–9 (2014).
26. Durst, J. *et al.* New insights into the electrochemical hydrogen oxidation and evolution reaction mechanism. *Energy Environ. Sci.* **7**, 2255–2260 (2014).
27. Hibiki, T. & Ishii, M. Active nucleation site density in boiling systems. *Int. J. Heat Mass*

Transf. **46**, 2587–2601 (2003).
28. Qi, Y., Klausner, J. F. & Mei, R. Role of surface structure in heterogeneous nucleation. *Int. J. Heat Mass Transf.* **47**, 3097–3107 (2004).
29. Qiu, Y. *et al.* Electrochemical Generation of Individual Nanobubbles Comprising H2, D2, and HD. *Langmuir* **36**, 6073–6078 (2020).
30. Kempler, P. A., Coridan, R. H., Lewis, N. S. & Lewis, N. S. Effects of bubbles on the electrochemical behavior of hydrogen-evolving Si microwire arrays oriented against gravity. *Energy Environ. Sci.* **13**, 1808–1817 (2020).
31. Janssen, L. J. J. Mass transfer at gas evolving electrodes. *Electrochim. Acta* **23**, 81–86 (1978).

Table of Contents Graphic